SDA Environmental Toolkit for Defense -- Enabling Space Environment and Weather Support for SDA Radar and Optical Sensors

Jeffery M. Cox
The Aerospace Corporation, Special Programs Division
Sage K. Andorka[1], Bryan L. Davis[1], Jennifer L. Benson[2]
(1) Space Systems Command, Space Domain Awareness Division (SSC/SZG),
(2) Air Combat Command, 2d Weather Squadron (557 WW/2 WS)

ABSTRACT

This paper describes the Space Domain Awareness (SDA) Environmental Toolkit for Defense (SET4D) migration of DoD space environment data and modeling capabilities to a GovCloud architecture. SET4D is modernizing the technology and capabilities to focus on space environment and weather impacts to SDA. Taking advantage of streamlined research-to-operations (R2O) and cloud architecture features, the Space Systems Command (SSC), contractor and federally funded research and development center team have developed and are operationalizing flowchart tools for a preliminary determination of hazards for SDA sensors. Previous work for space environment caused radio frequency hazards has been extended to include weather impacts on optical sensors including clouds, fog, aerosols, optical turbulence, meteors, and reflected solar light from the moon. The 24/7 Space Weather Operations Center in 2d Weather Squadron will be using these capabilities to provide real-time attribution and reach-back subject matter expertise to help SDA operators understand and mitigate environmental impacts.

1. SPACE DOMAIN AWARENESS (SDA) ENVIRONMENT TOOLKIT FOR DEFENSE (SET4D)

In April 2020, the Commander, USSPACECOM identified the enhancement of existing and development of new space domain awareness (SDA) capabilities as his command's number one priority. SDA is reliant on the fusion of space-focused Intelligence, Surveillance, Reconnaissance (ISR) and environmental monitoring. To address this priority, the Space Domain Awareness Environmental Toolkit for Defense (SET4D) is designed to be the United States Space Force (USSF) application suite for all space environment characterization and forecast information. Deployed in cloud-hosted environments, the SET4D goal is to operate on a self-service concept allowing for consumers of information to access customized workspaces for information as needed by the consumer. Data can be tailored to the consumer's mission needs, facilitating a more comprehensive depiction of the environment interaction within the mission envelope. Tailored alerting thresholds allow operators to work without requiring constant monitoring of the environment until necessary.

Serving the broader DoD, IC, and other government entities, SET4D's interface designs will accommodate all user's abilities while ensuring security of data and information through user roles. Access and user role definitions are managed by the Space Weather Flight (2WS/WXZ) at the 557th Weather Wing, who will be able to provide in-tool support for all users. Replicated baselines on three security enclaves (unclassified, Secret, and Top Secret--Sensitive Compartmented Information) will allow for exploitation of data available and full capability access by consumers in those enclaves.

2. SPACE ENVIRONMENT AND WEATHER HAZARDS

To enable rapid, repeatable attribution of environmental impacts to military systems, radio frequency links, and personnel, The Aerospace Corporation has prototyped and delivered several flowcharts to identify when location, time, geometry, and environmental observations can be used to rule out potential impacts. For the environment to be a cause of an impact, the location, time, geometry, along with the enhanced environment must all be hazardous.

Approved for public release. OTR 2022-00837.

Each flowchart's logic is designed to rule out the potential space environment and weather hazards by assessing the location of the impacted system, the time of the impact, the geometry of the field-of-view compared to the environment, and the environmental intensity [5].

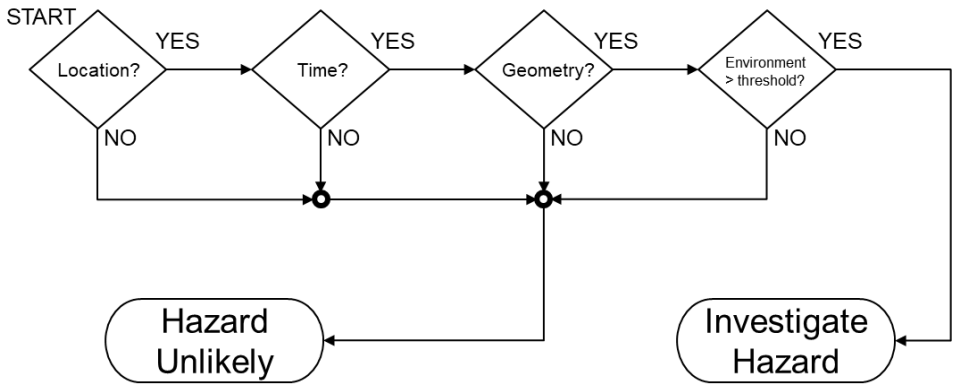

Fig. 1. Basic flowchart logic for space environment and weather impacts.

3. RADAR ELCTRO-MAGNETIC INTERFERENCE FLOWCHARTS

Following on from the previous development for SET4D that helped users relate the space environment and its impacts on DoD space missions, The Aerospace Corporation developed a set of flowcharts to address radar impacts from the environment. In this section, the paper will discuss the flowcharts designed to address electro-magnetic interference on radar links [3].

3.1 Radar Needs and Overview

The radar flowcharts are broken up into individual hazards for the impact event. The flowcharts are designed to provide a repeatable, rapid radar attribution for radio frequency (RF) signals attributable to environment hazards. In the nominal use case, the analyst is provided the time, location, frequency, and RF polarization of the potential radar impact, along with information about the RF transmission azimuth and elevation or the satellite being tracked. The analyst then collects data from various sources and executes the hazard flowcharts. The space environment and weather induced radar hazards are generically called <H>. Working through the appropriate flowchart results in a conclusion of "EMI Unlikely" or "Investigate <H>." In the former case, the preliminary determination is that hazard H is not the cause of the EMI/radar impact, and in the latter case, the preliminary determination is that hazard H is possibly the cause and should be investigated further. Each hazard is investigated separately, so there may be times when more than one hazard would need further investigation. The entire process from initiation to conclusion is expected to take the analyst 1-2 hours to manually complete the flowcharts.

3.2 Environmental Data for SDA Radar Flowcharts

In order to execute the SDA radar flowcharts, the analyst must collect space environment and tropospheric weather data from a variety of sources. The primary radar impact attribution data come from auroral model output, USSF radio telescopes, scintillation climatology, rain rate and atmospheric profile data.

3.3 SDA Radar Hazards

There are six environmental hazards covered by the SDA radar flowcharts, two caused by the space environment and four by tropospheric weather. The six hazards are auroral clutter/interference, equatorial scintillation, solar radio

burst radio frequency interference (RFI), meteor showers, rain fade, and anomalous propagation. Auroral clutter/interference is caused by plasma density irregularities in intense aurora. Scintillation is caused by electron density irregularities in the equatorial ionosphere. Solar RFI is caused by eruptive events on the Sun. Meteor showers cause interference when the radars are pointed near the radiant of intense showers. Rain attenuation for high frequencies is caused by absorption of RF signals in rain. Anomalous propagation, or ducting, is caused by temperature and humidity conditions in the troposphere.

3.3.1 Auroral Interference

Auroral clutter/interference is caused by back-scatter of RF off the plasma density irregularities in the auroral oval. The RF transmissions will reflect off of the aurora when the transmission path is perpendicular to the magnetic field and the particle precipitation causing the aurora is intense [19].

Auroral boundary modeling exploits the well-established relationship of equatorward and poleward expansion of the precipitating particles during increased geomagnetic activity [6], [7], [14], [16]. Empirical models of the auroral boundaries have been developed and used in operations for years to help specify the auroral locations in near real-time using only a geomagnetic index, K_p.

Johns Hopkins University Applied Physics Laboratory (JHU/APL) developed an auroral model based on far ultraviolet (FUV) data [22]. Global FUV observations by Thermosphere Ionosphere Mesosphere Energetics and Dynamics (TIMED)/Global Ultraviolet Imager (GUVI) are used to estimate the mean energy (E_o) and energy flux (Q) of precipitating electrons based on an auroral model and airglow Atmospheric Ultraviolet Radiance Integrated Code (AURIC) model [17]. The energy flux for 6 different, increasing geomagnetic activity levels have been calculated. GUVI measures the N_2 Lyman–Birge–Hopfield small (LBHS) 140.0–150.0 nm and Lyman–Birge–Hopfield long (LBHL) 165.0–180.0 nm auroral emissions. The Zhang and Paxton GUVI auroral model is a FUV-based and K_p dependent model of global auroral products (E_o, Q) and was developed using 4 years (2002–2005) of GUVI data. This FUV-based model covers all K_p ranges (0–9). The Zhang and Paxton GUVI auroral model equatorward and poleward latitudinal boundaries have also been determined for each magnetic local time (MLT) and K_p by defining the threshold 0.25 ergs/cm^2/s and are available for look-up in [3].

In addition to the empirical aurora models depending on geomagnetic activity indices, there have been successful auroral specifications based off solar wind velocity and magnetic field observations. This solar wind coupling to the hemispheric global power has led to the creation of the Oval Variation, Assessment, Tracking, Intensity, and Online Nowcasting – Prime (OVATION-Prime) model [15]. The OVATION-Prime auroral model is in operations at both NOAA and USSF and provides diffuse, monoenergetic and broadband auroral energy and number fluxes. Each type of aurora (i.e. diffuse, monoenergetic and broadband) is given a separate linear regression fit to the solar wind parameter which best predicts hemispheric global power [15]. This is necessary because each type of aurora responds differently to solar wind driving and because at different latitudes and different local times responses can be quite different.

Auroral clutter/interference is only possible in the auroral zone, so the flowchart's first check is to see if the E-Region ionospheric pierce point (E-IPP) is between the equatorward and poleward boundaries of the aurora when the intensity of the aurora is significant [21]. Then, the intensity of the auroral particle precipitation is examined from one of these two models (i.e. GUVI or OVATION-Prime) to assess the hazard.

3.3.2 Scintillation

Ionospheric scintillation is the rapid fluctuations of radio waves caused by small scale structures in the ionosphere. Severe scintillation conditions can degrade Satellite Communications (SATCOM), prevent a Global Positioning System (GPS) receiver from locking on to the signal, and cause interference on radars. Scintillation of radio waves impacts the power and phase of the radio signal. Scintillation is caused by small-scale (tens of meters to tens of km) structure in the ionospheric electron density along the signal path. Equatorial scintillation is confined to regions near the geomagnetic equator, within ±20° [20] and at local times from ~1 hour after sunset to ~1 hour before sunrise.

The analysis uses the F-region IPP to determine if the radar impact is within the equatorial region and the F-IPP MLT is between 19-05 LT. Frequencies above 2,400 MHz typically have negligible impacts from scintillation.

The occurrence rate of scintillation is proportional to the F-region electron density which is driven by solar emissions and modulates from high electron densities during solar maximum to lower electron densities during solar minimum. Additionally, there are longitudinal, seasonal, and geomagnetic activity effects that increase and decrease the likelihood of the development of an equatorial plasma bubble (EPB). JHU/APL used the GUVI data to characterize the occurrence rate of the EPBs from 2002-2006 (i.e. solar max-like conditions to solar min-like conditions) [2]. The flowchart uses a minimum EPB rate of 10% to conclude a result of "Investigate Scintillation."

3.3.3 Solar Radio Frequency Interference

Solar RFI is caused by radio frequency noise generated on the sun during large solar flares. Solar radio bursts were discovered during WWII due to impacts on Allied radars and communications. During explosive events on the sun, radio bursts of significant intensity can overwhelm receivers with RFI. Any communication, navigation, or radar system on the sun-lit side of the Earth can be affected, but when the geometry of the receiver is such that the transmitter and sun are in conjunction, the impact can be severe. The conjunction angle, θ, between the azimuth and elevation of the radar/SATCOM antenna and sun is given by,

$$\theta = \cos^{-1}(\sin LAT \sin LAT_{SSP} + \cos LAT \cos LAT_{SSP} \cos(LON - LON_{SSP})) \quad (1)$$

The flowchart considers any conjunction angles ≤ 45° to capture the main lobe and primary side lobes of the antenna and to be hazardous.

The USSF Radio Solar Telescope Network (RSTN) observatories at Sagamore Hill, MA, Keana Point, HI, Learmonth, Australia and San Vito, Italy operate the AN/FRR-95 Radio Interference Measurement Set (RIMS) on eight discrete frequencies using 3 antennas. The solar observatories report significant radio bursts within 2 minutes of occurrence. The 2d Weather Squadron (2 WS) issues the WOXX-52 bulletin to warn radar operators of potential solar RFI for an observed radio burst. By simply choosing the closest frequency and determining the solar conjunction of the radar receiver, the potential solar RFI impact can be assessed for a radar impact event.

3.3.4 Meteor Showers

Meteors are pieces of dust and debris from space that burn up in Earth's atmosphere, where they can create bright streaks across the night sky and emit radio frequencies that can be misinterpreted as missiles or satellites. The meteor shower flux is forecast annually by NASA's Meteoroid Environment Office using the standard double-exponential shape of a meteor shower activity profile. Meteor shower models [13] are based off the population index and include an approximate sporadic background [11]. The sporadic background is much less well understood and parameterized than the showers but can add an appreciable amount to the shower meteor rates. The Zenith Hourly Rate (ZHR) describes the rate at which a meteor shower produces visible meteors at magnitude +6.5 brightness.

In order for the meteor shower to be able to cause radar impacts, the meteor radiant must have an elevation and azimuth in the radar's field-of-view and be above the horizon. To determine the conjunction angle of the meteor shower radiant and the ground-based radar, we use an equation similar to (1), but with the azimuth/elevation of the radar and radiant,

$$\theta = \cos^{-1}\big((\sin EL_R \sin EL) + (\cos EL_R \cos EL \cos(AZ - AZ_R))\big) \quad (2)$$

where the subscript R represents the radiant elevation (EL_R) and azimuth (AZ_R).

3.3.5 Rain Attenuation

Rain fade or attenuation is caused by the absorption of a radio frequency signal by atmospheric rain. The International Telecommunication Union (ITU) Radiocommunication Sector (ITU-R) has determined the specific attenuation due to rain losses, γ_R. ITU-R Recommendations is the name given to the set of international technical standards developed by the ITU-R. These Recommendations are the result of studies undertaken by Radiocommunication study groups. ITU-R recommendation P.838 provides experimentally estimated specific attenuation given the frequency, polarization, rain rate and elevation angle [9].

The experimental data for specific attenuation in units of dB/km caused by liquid precipitation takes on a Power law relationship,

$$\gamma_R = kR^{\alpha} \tag{3}$$

with rain rate, R, given in mm/hr. The Power Law parameters are,

$$k = [k_H + k_V + (k_H - k_V)\, cos^2\, EL\, cos\, 2\tau]/2 \tag{4}$$

$$\alpha = \ [k_H\alpha_H + k_V\alpha_V + (k_H\alpha_H - k_V\alpha_V)\, cos^2\, EL\, cos\, 2\tau]/2k \tag{5}$$

where EL is the elevation angle and τ is the polarization tilt angle relative to the horizontal ($\tau = 45°$ for circular polarization). If the analyst does not know the polarization, assume circular polarization. The horizontal and vertical polarized coefficients, k_H and α_H, and k_V and α_V, respectively, for a given frequency are listed in [9].

The absolute rain fade (dB) can be determined if the rain cell volume along the RF link path is known. See [1], the average horizontal rain cell sizes were determined by analyzing three years (i.e. 240,000) of rain cells and determined to fit the simple relationship of 3.3R-0.08 and range from 3.1-2.3 km for light rain to tropical rain. The vertical extent/thickness of rain varies from <1 km to 5 km thickness as rain rate increases from 2.5-100 mm/hr. Consequently, using specific attenuation of 1 dB/km would lead to typical fades of ~3 dB (50% loss) for low elevation RF links in downpours and tropical rain for isolated cells and more attenuation for widespread convection with numerous cells along the RF link.

In order to calculate the absolution attenuation, multiply the specific attenuation by an estimate of the path length through the rain. The simple assumption that the RF link's path through the rain is from the ground site to the freezing level, above which the water is frozen and not causing the attenuation from Equation 3. The path length to the freezing level, $PL_{0°}$, will be defined by the elevation angle and the freezing level height above the ground, $AGL_{0°}$.

$$PL_{0°} = \frac{AGL_{0°}}{\sin EL} \tag{6}$$

In the event the user is unable to access model data for freezing level heights, National Centers for Environmental Prediction (NCEP) reanalysis and comparison to Tropical Rainfall Measuring Mission (TRMM) satellite data can be used to estimate the freezing level heights for tropical, mid-latitudes and polar latitudes [8].

3.3.6 Anomalous Propagation and Ducting

Anomalous propagation or ducting of active radar signals is caused by temperature and humidity conditions in the atmosphere. The International Telecommunication Union (ITU) Radiocommunication Sector (ITU-R) has determined the refraction of radiowaves is controlled by the refractivity index, *N* [10]. By assessing the vertical refractivity gradient (ΔN/km) of the atmosphere above the radar site, the user can determine the propagation characteristics of Very High Frequency (VHF) and Ultra High Frequency (UHF) radiowaves.

The refractivity index, *N*, is defined by

$$N = \frac{77.6}{T}\left(P + 4810\frac{e}{T}\right) \tag{7}$$

where T is the temperature (K), P is the total atmospheric pressure (hPa) and e is the water vapor pressure (hPa). The water vapor pressure is calculated using the saturation vapor pressure (e_s) and relative humidity (H),

$$e = \frac{H \cdot e_s}{100} \tag{8}$$

and the saturation vapor pressure (e_s) is defined by,

$$e_s = EF_{water} \cdot 6.1121 \cdot exp\left[\frac{\left(18.678 - \frac{T}{234.5}\right) \cdot T}{T + 257.14}\right] \tag{9}$$

where T is the temperature (°C), valid from -40° to +50°C. The specific emission factor (EF) of water is defined as,

$$EF_{water} = 1 - 10^{-4}[7.2 + P \cdot (0.0320 + 5.9 \cdot 10^{-6} \cdot T^2)] \tag{10}$$

where P is the total atmospheric pressure (hPa) and T is the temperature (°C). Finally, using the vapor pressure, temperatures, and isobaric pressures in Eq. (14) yields the refractivity index in "N units." The refractive index must be computed at each height and then the refractivity gradient can be computed between adjacent heights. By assessing the vertical refractivity gradient (ΔN/km), one can determine the atmospheric propagation characteristics; if the vertical refractivity gradient is <-157 then ducting is likely.

4. OPTICAL HAZARD FLOWCHARTS

Following on from the previous development for SET4D that helps users relate the space environment and its impacts on DoD missions, The Aerospace Corporation developed a set of flowcharts to address optical impacts from the environment. In this section, the paper will discuss the flowcharts designed to address environmental hazards on optical sensors [3].

4.1 Optical Needs and Overview

The optical flowcharts are broken up into multiple hazards. The flowcharts are designed to provide a repeatable, rapid attribution for visible and infrared wavelength obscurants to environment hazards. In the nominal use case, the analyst is provided the time and location of the optical impact, along with information about the azimuth and elevation of the sensor or the satellite being tracked. The analyst then collects data from various sources and executes the flowcharts. The flowcharts include different space environment and weather induced optical hazards generically called <H>. Working through the appropriate flowchart results in a conclusion of "Visible Hazard Unlikely" or "Investigate <H>." In the former case, the preliminary determination is that hazard H is not the cause of the obscurant, and in the latter case, the preliminary determination is that hazard H is possibly the cause and should be investigated further. The entire process from initiation to conclusion is expected to take the analyst 1-2 hours [5].

4.2 Environmental Data for SDA Optical Flowcharts

In order to execute the SDA optical flowcharts, the analyst must collect space environment and tropospheric weather data from a variety of sources. The primary optical attribution data come from numerical weather model output, plus data from aerosol models, meteor shower times/radiants, and geometry calculations of sensor fields-of-view.

4.3 SDA Optical Hazards

There are seven environmental hazards covered by the SDA optical flowcharts. The weather/surface condition causes four and the sensor field-of-view geometry causes three hazards. The seven hazards are clouds, optical turbulence, aerosols, meteor showers, sun-in-sensor, glint, and moon-in-sensor. Clouds and fog prevent SDA optical observations by blocking the light from the resident space objects (RSOs). Optical turbulence is caused by temperature gradients and wind shear. Aerosol obscurants from smoke, dust and ash are tracked as hazards. Similar to radar impacts, meteor showers can also be misinterpreted as satellites or missiles. Sun illumination of space-based sensors or reflected by the moon for ground-based sensors are also hazards (sun-in-sensor and moon-in-sensor, respectively). Finally, glint is surface reflected solar illumination into space-based sensors. Glint is only a hazard when the surface or atmosphere has a high albedo (i.e., clouds, snow, ice, and calm water) [5].

4.3.1 Clouds

Obviously, clouds above a ground-based optical sensor are a significant hazard to SDA capabilities. For this optical hazard capability, we consider any fog (visibilities < 10 miles) and any clouds to be an issue. Numerical weather prediction model outputs of surface visibility and cloud water for the entire atmosphere have been used to determine the occurrence of obscurants.

4.3.2 Optical Turbulence

Optical turbulence can have a significant impact on a ground-based optical sensor's sensitivity. The optical turbulence intensity is driven by the temperature gradient and wind shear in the atmosphere above the telescope. To specify the optical turbulence, we use the refractive index structure parameter, C_n^2. Estimation models that convert standard meteorological data of pressure, temperature, and wind speed into C_n^2 vertical profiles are established based on the basic theory of turbulence [18];

$$C_n^2 = 2.8\, L_0^{4/3} M^2 \tag{11}$$

$$M^2 = \left[\frac{-79\times10^{-6}P}{T}\frac{\partial \ln\theta}{\partial z}\right]^2 \tag{12}$$

$$\theta = T\left(\frac{1000}{P}\right)^{0.286} \tag{13}$$

$$L_0^{4/3} = 0.1^{4/3} \times 10^{0.362+16.728\,S-192.347\frac{\partial T}{\partial z}} \tag{14}$$

$$S = \sqrt{\left(\frac{\partial u}{\partial z}\right)^2 + \left(\frac{\partial v}{\partial z}\right)^2} \tag{15}$$

where pressure P (unit: hPa) and temperature T (unit: K), and vertical wind shear S is defined by the U and V components of the horizontal winds.

4.3.3 Aerosols

Similar to clouds, aerosols in the atmosphere above the ground-based optical sensors can obscure the spacetrack objects and limit detection and tracking capabilities. Aerosols come in several categories, e.g., smoke, dust, and volcanic ash. Anytime the aerosol optical depth is elevated, as measured and modeled by International Cooperative for Aerosol Prediction (ICAP) Multi-Model Ensemble, smoke and dust will be a hazard. The major sources of smoke and dust come from forest fires or agricultural biomass burns and from desert dust, respectively. For volcanic ash, the developed hazard flowchart uses the proxy of sulfur dioxide (SO_2) concentration observations for NOAA satellites. SO_2 gases are released from volcanic eruptions along with the ash.

4.3.4 Meteor Showers

See section 3.3.4, Eq 2 for calculating the conjunction angle between the optical sensor's field-of-view and the meteor shower radiant, to be a hazard the meteors must be in the field-of-view [4].

4.3.5 Sun-in-Sensor for Satellite Sensors

During seasons near Equinox, optical sensors on GEO satellites near midnight local time can have solar illumination intrusion into sensors, this is called sun-in-sensor. In order to calculate the hazard, the analyst will use the LAT/LON of the satellite and anti-sub-solar point (assp) to determine the solar nadir angle [4].

$$\varphi = \cos^{-1}\left[sin\, LAT_{sat}\, sin\, LAT_{assp} + cos\, LAT_{sat}\, cos\, LAT_{assp}\, cos\left(LON_{sat} - LON_{assp}\right)\right] \quad (16)$$

when the solar nadir angle, which is the central angle difference between the assp and the sub-satellite point (satellite's LAT/LON), is ≤ 15° then sun-in-sensor hazard is likely. This equates to approximately within 37 days of Equinox and within 60 minutes of midnight.

4.3.6 Solar Illumination Glint from Orbit

For solar illumination glint to be an SDA hazard two conditions must be met; the glint location must be a location of high surface albedo (e.g. water, snow, or ice) and the geometry of the sun, location and satellite must be aligned so that the relative glint angle is small. The relative glint angle is defined by the elevation and azimuth of the sun and satellite. For the relative glint angle to be small, the elevations of the sun and satellite must be approximately equal, and the azimuth of the sun and satellite differ by approximately 180°, see Figure 2 [4].

To determine the relative glint angle, ϕ,

$$\cos\phi = (cos\,\chi\, cos\,\theta) + \left(sin\,\chi\, sin\,\theta cos\left(\pi - (AZ_{sat} - AZ_{sun})\right)\right) \quad (17)$$

where χ is the solar zenith angle, θ is the zenith angle of the satellite (i.e. complementary to the satellite's elevation angle) and AZ_{sat} and AZ_{sun} are the azimuth of the satellite and sun from the glint location with respect to North, respectively. If the relative glint angle, ϕ is > 0 and ≤ 36°, then glint is possible depending on the surface reflectivity.

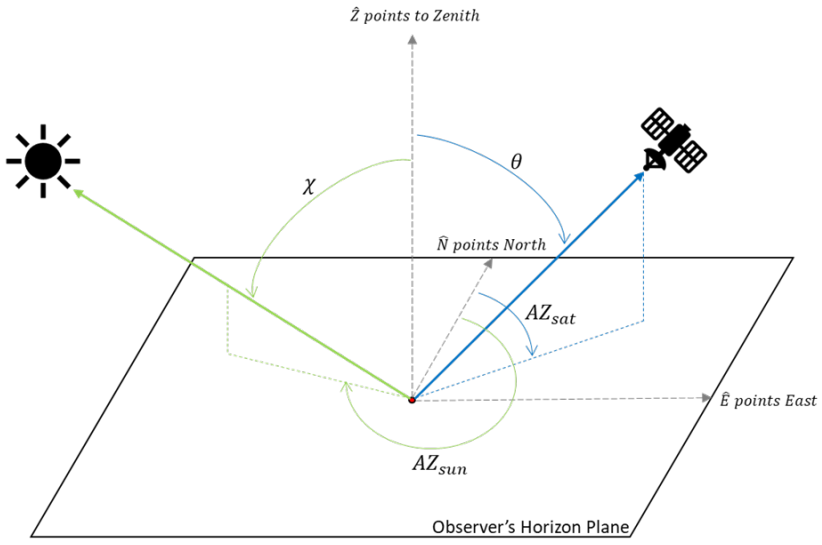

Fig. 2. Illustration of relative glint angle geometry.

The determination of high albedo is controlled by the surface condition types of clouds, water, snow, or sea ice of any concentration. In other words, dry land has a low albedo and will not cause glint, while snow covered land, relatively calm water, and ocean with any amount of ice concentration can cause glint.

4.3.7 Moon-in-Sensor

Ground-based optical sensors can be effectively blinded by sunlight reflected off the moon. We call this hazard, "moon-in-sensor" and it is dependent on the lunar elevation, phase, and conjunction angle. The moon's elevation and phase can be calculated by the time and ground-based sensor location [12].

The declination (δ) and right ascension (α) of the Moon for a given time provides the hour angle, which in turn can be used to calculate the optical sensor's lunar elevation and azimuth.

$$\mathrm{EL}_{Moon} = \sin^{-1}(\sin\delta_{Moon}\ \sin LAT + \cos\delta_{Moon}\cos LAT\cos HA) \tag{18}$$

$$\mathrm{AZ}_{Moon} = \tan^{-1}(\sin HA\,, \cos HA\sin LAT - \tan\delta_{Moon}\cos LAT) \tag{19}$$

Finally, the conjunction angle of the moon (θ_M) must be such that the optical sensor is looking towards the moon for this to be a hazard, Eq 1 is modified to;

$$\theta_M = \cos^{-1}\big((\sin EL_{Moon}\sin EL) + (\cos EL_{Moon}\cos EL\cos(AZ - AZ_{Moon}))\big) \tag{20}$$

5. 2d WEATHER SQUADRON OPERATION

The 557th Weather Wing includes the 2d Weather Squadron (2 WS) that has the mission of observing solar emissions around the globe at solar observatories and operating the 24/7 Space Weather Operations Center (SpWOC). The SpWOC provides warnings, and both general and customized products to help DoD operators determine space environment impacts. As the SET4D capabilities get developed and operationalized on the GovCloud, 2 WS will focus their efforts on providing reach-back subject matter expertise, customer coordination, tailored forecasting, and detailed deep-dive analyses.

6. FUTURE WORK

Future work in support of SDA environmental hazards should include specific thresholding, sensitivity analyses, and forecasting these hazards. The current work is mostly focused on ruling out the environment and not determining the level of impact or predicting the likelihood of impacts in the future. If successful forecast of mission impacting hazards can be established, then the SDA operations can plan around these impacts and mitigate the effects.

7. SUMMARY

To address the critical need for environmental attribution of impacts on SDA optical and radar systems, The Aerospace Corporation, in collaboration with Space Systems Command and 2d Weather Squadron, developed flowcharts to eliminate the environment when the location, frequency, geometry, and environment are non-hazardous. Data from weather and space environment observations and models are exploited to make these rapid, repeatable attributions.

8. REFERENCES

[1] Crane, Robert K. (1982), A two component rain model for the prediction of attenuation statistics, Radio Sci., 1982, 17, 1371-1387.

[2] Comberiate, J., and L. J. Paxton (2010), Global Ultraviolet Imager equatorial plasma bubble imaging and climatology, 2002–2007, J. Geophys. Res., 115, A04305, doi:10.1029/2009JA014707.

[3] Cox, J.M., T.P. O'Brien, A. J. Boyd and D. G. Brinkman (2021), A human-in-the-loop decision tool for preliminary assessment of the relevance of the space environment to electro-magnetic interference, Aerospace Report Number TOR-2021-00972, The Aerospace Corporation, El Segundo, CA, Mar 12, 2021.

[4] Cox, J.M., T.P. O'Brien, A. J. Boyd and L.J. Gelinas (2021), A human-in-the-loop decision tool for preliminary assessment of the relevance of the space environment and weather conditions to Launch and Predicted Impacts, Aerospace Report Number TOR-2021-01499, The Aerospace Corporation, El Segundo, CA, June 25, 2021.

[5] Cox, J. M., T. J. Kopp, J. P. Subasavage (2022), Aerospace Study on Space Domain Awareness (SDA) Environmental Toolkit for Defense (SET4D) - Environmental Impacts Attribution, Determination, and Calculations, Aerospace Report Number TOR-2022-00600, The Aerospace Corporation, El Segundo, CA, Feb 2, 2022.

[6] Gussenhoven, M. S., D. A. Hardy, and N. Heinemann, (1983), Systematics of the Equatorward Diffuse Auroral Boundary, J. Geophys. Res., 88, pp. 5692-5708.

[7] Hardy, D. A., M. S. Gussenhoven, and E. Holeman (1985), A Statistical Model of Auroral Electron Precipitation, J. Geophys. Res., 90, 4229-4248.

[8] Harris, G. N., K. P. Bowman and D-B Shin, (2000), Comparison of freezing-level altitudes from the NCEP reanalysis with TRMM precipitation radar Brightband data, J. Clim., 13, 4137–4148.

[9] ITU-R P.838-3 (2005), Specific attenuation model for rain for use in prediction methods.

[10] ITU-R P.453.14 (2019), The radio refractive index: its formula and refractivity data.

[11] Jenniskens, P. (1994), Meteor stream activity, I. The annual streams, Astronomy and Astrophysics, 287, 990-1013 (1994).

[12] Meeus, J., 1998, Astronomical algorithms, 2nd ed., ISBN 0-943396-61-1, chapters 47.

[13] Moorhead, A. V., et al., (2019), Meteor shower forecasting in the near-Earth space, Journal of Spacecraft and Rockets, doi:10.2514/1.A34416.

[14] Newell, P. T., T. Sotirelis, J. M. Ruohoniemi, J. F. Carbary, K. Liou, J. P. Skura, C.-I. Meng, C. Deehr, D. Wilkinson, and F. J. Rich (2002), OVATION: Oval variation, assessment, tracking, intensity, and online nowcasting, Annales Geophysicae 20: 1039–1047.

[15] Newell, P. T., T. Sotirelis, K. Liou, C.-I. Meng, and F. J. Rich (2007), A nearly universal solar wind-magnetosphere coupling function inferred from 10 magnetospheric state variables, J. Geophys. Res., 112, A01206, doi:10.1029/2006JA012015.

[16] Newell, P. T., T. Sotirelis, and S. Wing (2009), Diffuse, monoenergetic, and broadband aurora: The global precipitation budget, J. Geophys. Res., 114, A09207, doi:10.1029/2009JA014326.

[17] Strickland, D.J., Bishop, J., Evans, J.S., Majeed, T., Shen, P.M., Cox, R.J., Link, R., Huffman, R.E., (1999), Atmospheric ultraviolet radiance integrated code (AURIC): theory, software architecture, inputs, and selected results. Journal of Quantitative Spectroscopy & Radiative Transfer 62, 689.

[18] Tatarski, V.I.; Silverman, R.A.; Chako, N., Wave Propagation in a Turbulent Medium. Phys. Today 1961, 14, 46.

[19] Tsunoda, R. T. (1991), Auroral-Clutter Predictions for Flyingdales, England, PL-TR-911-2198.

[20] Whalen, J.A. (1997), Equatorial bubbles observed at the north and south anomaly crests: Dependence on season, local time, and dip latitude, Radio Science, Vol 32, Number 4, Pages 1559-1566, July-August 1997.

[21] Zhang, Y., E.J. Mitchell, E.S. Miller, J. Comberiate, R.K. Schaefer and L. Paxton (2018), Personal Conversation with JHU/APL, Sep 7, 2018.

[22] Zhang, Y., and L. Paxton (2008), An empirical Kp-dependent global auroral model based on TIMED/GUVI FUV data, JASTP 70 (2008) 1231–1242.